Title
THE OXIDATION OF ALUMINA FORMERS IN AIR AND LOW PO2 ATMOSPHERE

Authors
Miner, R.G.
Nagarajan, V.

Publication Date
1980-08-01

LBL-11379 c.2
Preprint

Lawrence Berkeley Laboratory
UNIVERSITY OF CALIFORNIA

Materials & Molecular Research Division

Submitted to Oxidation of Metals

THE OXIDATION OF ALUMINA FORMERS IN AIR AND LOW P_{O_2} ATMOSPHERE

Robert G. Miner and Vaidyanathan Nagarajan

August 1980

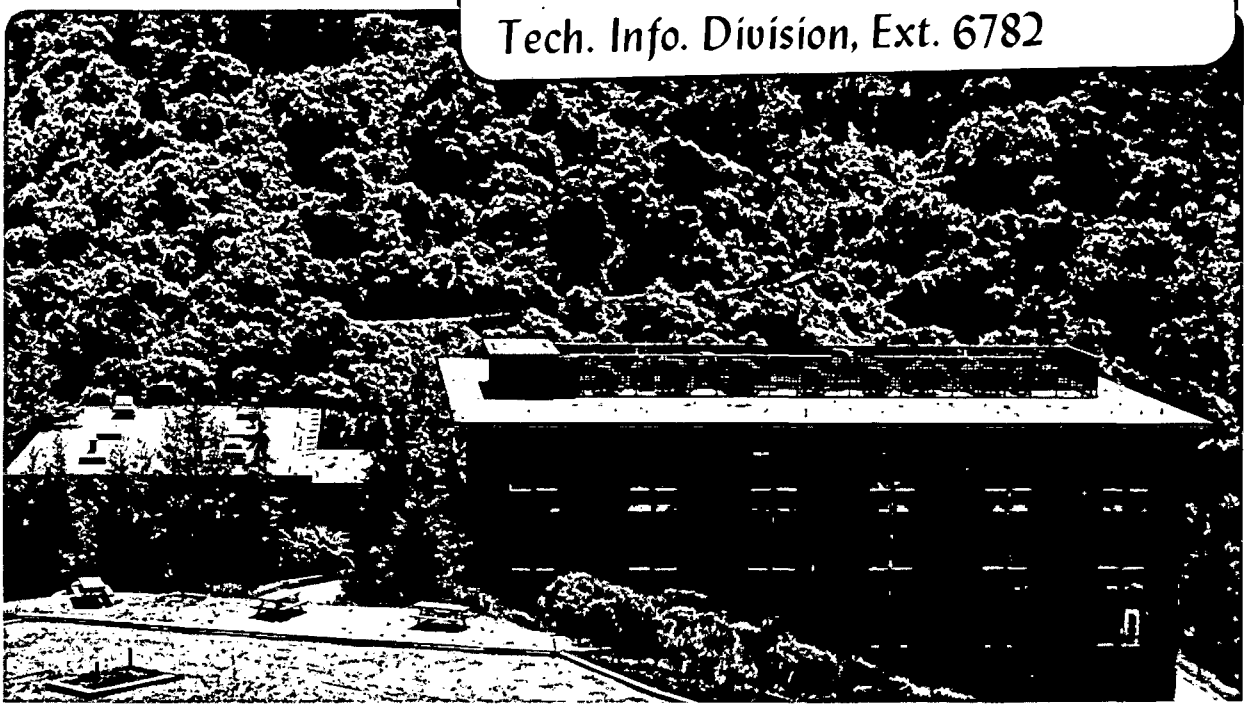

Prepared for the U.S. Department of Energy under Contract W-7405-ENG-48

DISCLAIMER

THE OXIDATION OF ALUMINA FORMERS IN AIR AND LOW P_{O_2} ATMOSPHERE

Robert G. Miner* and Vaidyanathan Nagarajan**
Materials and Molecular Research Division, Lawrence Berkeley Laboratory
University of California, Berkeley, CA 94720

September, 1978

ABSTRACT

The oxidation behavior of a series of iron-base alloys was studied at a temperature of 982°C (1800°F) and in a low P_{O_2} environment. Weight change measurements were made and the morphology of the oxide scales were examined using optical metallography and scanning electron microscopy. It was determined that alloys of composition Fe-18Cr-(3-5)Al that formed a duplex, layered Cr_2O_3 on Al_2O_3 scale had the best scaling resistance.

Key words: alumina formers, oxide morphology, oxide scale adherence, internal precipitation

---

*Presently with the General Electric Company, Cincinnati, Ohio.
**Presently with Battelle Columbus Laboratories, Columbus, Ohio.

INTRODUCTION

Iron-base alloys such as 310 stainless steel and Incoloy 800 are candidate alloys for use as internal components in the elevated temperature regions of coal gasifiers.[1] These alloys contain large amounts of chromium which is generally accepted as a requirement for elevated temperature corrosion resistance[2]. In coal gasifiers the atmosphere can be very corrosive at operating temperatures of 538°C to over 1000°C[3] and pressures, atmospheric to about 1500 psi[4], with sulfur and oxygen being the two most aggressive constituents[5]. Because Cr_2O_3 is not a sufficient barrier to sulfur and in view of the strategic importance of chromium, it is important that the level of chromium be reduced while improving the sulfidation resistance of alloys for coal gasifier service. Acceptable corrosion barrier replacements for Cr_2O_3 are SiO_2 and Al_2O_3. Both oxides have high melting points, relatively high negative free energies of formation close to stoichiometric composition, and low diffusion coefficients for both cations and anions which are not adversely affected by impurities.

The use of SiO_2 as a barrier layer to the diffusion of oxygen and sulfur at elevated temperature should be avoided since its reduction to the volatile SiO may occur. Also SiO_2 may react with other metallic ions to form complex molten oxides[6]. Problems also exist with the use of Al_2O_3 which, hopefully, can be overcome by alloy design. First, Al_2O_3 scales have poor adherence during thermal cycling[7] and, second, Al additions to the base alloy in the quantity required to produce a barrier layer may reduce the melting point and the certain desirable properties of the alloy to unacceptable levels[8]. The addition of an oxygen getter

such as chromium to the Fe-Al system presents one way of lowering the aluminum concentration below a level where the mechanical and physical properties of the alloy are not degraded[9, 10]. Thus, this study reports the results of an investigation of the oxidation behavior of a series of experimental Fe-Cr-Al alloys. Specifically, the surface morphology of the Al_2O_3 oxide and the cross-section morphology of the alloys that were oxidized in air, P_{O_2} = .2 atm, and in a low P_{O_2} environment, $P_{O_2} = 10^{-18}$ atm, without sulfur present, at 982° C (1800°F) were investigated.

EXPERIMENTAL PROCEDURES

The material used in this investigation was melted in an induction furnace under an argon atmosphere, then cast into five-pound ingots, and subsequently homogenized at 1200°C for 24 hours. The casting was forged and flat-rolled into thin sheets from which test coupons measuring 1.5 cm x 1.5 cm x .1 cm were machined. Chemical analysis to determine the composition (in wt %) was performed and these compositions are listed in Table I. Each specimen was polished using wet silicon carbide abrasive paper through 600 grit. Having thoroughly washed the surfaces of each specimen with soap solution, distilled water, and ethanol, the dimensions of the specimens were determined using a micrometer to the nearest 0.005 cm. Prior to oxidation the weight of each was recorded to the nearest 0.002 gm.

The air oxidation tests were run at 982°C (1800°F) in laboratory air using either a horizontal tube furnace or a box-configuration furnace. The method of inserting the test coupons into the heat zone differed according to the furnace type. The horizontal tube furnace required that

the test samples be slowly introduced and removed from the hot zone, whereas the box furnace allowed the test samples to be inserted and removed without delay. Oxidation durations lasted one, three, five and nine days. After exposing the alloys for the required duration, the test coupons were removed from the furnace and weighed on a balance for one measurement of the extent of oxidation.

Oxidation in the low P_{O_2} atmosphere was performed in a vertical tube furnace. Predetermined amounts of water vapor and hydrogen were introduced into the oxidation furnace by passing argon gas through a column of water. The equilibrium established between H_2, O_2, and H_2O enabled the P_{O_2} to be maintained constant at 10^{-18} atm. Oxidation in the H_2O/H_2 environment lasted three days.

The morphologies of the resultant oxide and metal surfaces and cross sections were examined in the AMR-1000 Scanning Electron Microscope equipped with an energy dispersive analysis of x-ray (EDAX) unit. Accelerating voltage was 20 kV. Phase analysis was performed with a Norelco x-ray diffractometer using CuK_α radiation.

RESULTS

A. Growth Kinetics

Figure 1 a, b shows the weight gain data obtained over duplicate runs for the Fe-Cr-Al and Fe-10Al alloys oxidized in air for one, three, five and nine days. As seen, the rate decreased with time for all alloys. Due to the manner in which this weight gain data was measured, after removal of the specimens from the furnace with cooling to room temperature, it is emphasized that the results are qualitative, and only serve to show

general trends. Fe-10Al with 5 wt % chromium greatly increased the weight gain over that of the base Fe-10Al alloy. Further increases in the chromium content, Figure 1b, lowered the weight gain values. The Fe-18Cr-3Al and Fe-18Cr-5Al alloys showed nearly identical weight changes.

B. Surface Scale Morphologies

On removal from the furnace, the samples were covered by a white, single, thin surface oxide layer. Using x-ray techniques described elsewhere, the scales were found to be α-Al_2O_3. Upon cooling these alloys from the test temperature, the Al_2O_3 film readily spalled and, in some instances, was lost.

The oxide scales that formed on the Fe-18Cr-3Al and Fe-18Cr-5Al alloys were more adherent than those scales formed on the others. The loss of oxide scale from the alloy substrate presented a considerable problem in obtaining accurate kinetic data. The oxide film grown on the binary Fe-10Al alloy was the least adherent. This may explain the very low weight gain values measured for the binary alloy.

The morphology of the oxide that enveloped the Fe-Cr-Al alloys depended on the type of furnace and the oxygen partial pressure. In general, the oxide structure was either wrinkled, spaghetti-like, or smooth and compact. The latter morphology was more prevalent on those samples oxidized in the box furnace or in the low P_{O_2} atmosphere where the alloys were introduced into the hot zone without delay. The former structure was found on those samples oxidized in the horizontal tube furnace where the method of inserting the specimens was much slower. The wrinkled Al_2O_3 scales were prone to spall on cooling from the test temperature.

Figure 2a shows the oxide morphology formed on the Fe-18Cr-7Al alloy after five days. This oxide structure is typical of the spaghetti-like, or corrugated, morphology. The direction of the ridges of oxide texture may have indicated the direction of polishing. One region where the wrinkled oxide partially spalled from the Fe-18Cr-7Al substrate was photographed, Figure 2b. Ribbons of complex oxide decorated the alloy surface. These oxides served to key the surface oxide layer to the alloy substrate.

On those alloys that developed a relatively compact and smooth layer of Al_2O_3, the scales were decorated with nodules of aluminum oxide (Figure 3). Again, the texture of the oxide seemed to indicate the direction of polishing. This surface layer contained small amounts of chromium and iron. The spaghetti-like structure, however, was pure Al_2O_3. In some cases, on the surfaces of the air oxidized Fe-(5-10)Cr-10Al alloys, iron-rich nodules of oxide were observed protruding through the surface Al_2O_3 scale.

Whenever the spaghetti-like oxide structure was observed, the morphology was similar. The binary alloy, Fe-10Al alloy, however, showed a more convoluted structure. Figure 4 compares the features of the oxide morphology developed on the binary Fe-10Al (Figure 4a), Fe-10Cr-10Al (Figure 4b), and Fe-18Cr-3Al (Figure 4c) alloys during air oxidation.

On some samples there were regions which were covered by Al_2O_3 scales at temperature that spalled off on cooling, enabling the alloy surface beneath the scale to be examined. Figure 5 depicts one area of a Fe-5Cr-10Al alloy surface where the scale detached, exposing a region marked by corrugations and small, smooth depressions. Identical features

were noted on other alloys exposed in air and in the low P_{O_2} environment where spalling of the scale had occurred.

The oxide morphology that formed on the Fe-10Al alloy depended only on the oxygen partial pressure of the environment. In air the scale appeared as an interwoven conglomeration of aluminum oxide spaghetti, Figure 6a. The ballooned and convoluted structure of Al_2O_3 appeared hollow. In the low P_{O_2} environment, Fe-10Al developed a fine granular texture of Al_2O_3 (Figure 6b). In both atmospheres there appeared nodular growths of iron-rich oxide which protruded through the surface Al_2O_3 scale.

C. Metallographic Examination of Cross-Sections

In cross-section the Fe-(5-15)Cr-10Al alloys showed internal formations of Al_2O_3 inclusions after exposure in air and the low P_{O_2} atmosphere. Whether the experiments were performed in the box furnace or the tube furnace did not affect the formation of internal Al_2O_3 inclusions. The depth to which the Al_2O_3 inclusions penetrated the metallic core depended more on the chromium concentration than on the oxygen partial pressures of the atmosphere, the extent decreasing with increasing chromium and decreasing oxygen activities. Inclusion penetration appeared insensitive to the length of exposure. Figures 7 a and b are optical micrographs depicting the scale-alloy interface of Fe-5Cr-10Al and Fe-15Cr-10Al, respectively, after exposure in air for five days. Comparing these two figures, the depth of penetration is seen to decrease with increasing chromium content.

Scanning electron micrographs comparing the scale-alloy interface developed on the Fe-(5, 10, 15)Cr-10Al alloys after oxidation in the box

furnace and tube furnace are shown in Figures 8a and b, respectively. As is shown in Figure 8a, the scale which formed on the alloy in the box furnace remained adherent despite the uneven and undulating metallic surface. Precipitates of Al_2O_3 were present below the scale in the metal interior. The scales formed on the Fe-Cr-10Al samples in the tube furnace, Figure 8b, were not always attached to the metal substrate, and internal precipitates of Al_2O_3 were absent in the detached regions. Internal oxide inclusions were never observed in the Fe-18Cr-(3-5)Al alloys regardless of the type furnace, duration of exposure, or oxygen partial pressure. Nevertheless, the scale on these alloys appeared fairly adherent.

The interior of the air-oxidized specimens of Fe-10Al alloy did not contain internal inclusions of oxide. The ballooned and convoluted oxide structure is shown in Figure 9. As seen, the multiple layers of Al_2O_3 covered the metallic substrate.

After exposure for three days in the low P_{O_2} atmosphere, the Fe-10Al alloy showed massive internal oxidation. Within the metal interior, oxidation of aluminum occurred along grain boundaries of the alloy. Figure 10 shows a secondary electron image of a region where massive oxidation occurred. The X-ray maps show the internal distribution of the oxidation products. These oxides were found to be aluminum-rich. Islands of unreacted metal, which are depleted in the aluminum, are seen embedded in the oxide. Figure 11 shows the scanning electron micrograph and the iron and aluminum x-ray maps of a region containing islands of unreacted metal.

DISCUSSION

In simple binary alloys of Fe-Al, 7 wt % aluminum is needed to form a protective external scale of Al_2O_3.[11] At lower concentrations of aluminum, other complex aluminum-iron oxides can form, in addition to Al_2O_3. It has been observed that when chromium (10-15 wt % or higher) is alloyed with Fe-Al, the aluminum level required for continuous Al_2O_3 formation is only 3-5 wt %.[12] The oxidation mechanisms operating in the case of Fe-Cr-Al alloys is well known and is discussed elsewhere [13, 14, 15]. Chromium reduces the entry of oxygen into the alloy, thereby promoting a complete external Al_2O_3 layer rather than its precipitation as internal oxide[9].

The Fe-18Cr-3Al and Fe-18Cr-5Al alloys demonstrated excellent scaling resistance in air. Their superior oxidation resistance is attributed to the presence of a protective duplex Cr_2O_3-Al_2O_3 scale[16]. The mechanism of formation of this duplex scale is discussed elsewhere[17]. Chromium reduces the entry of oxygen into the alloy, thereby promoting a complete external Al_2O_3 layer, rather than its precipitation as internal oxide. The formation of iron oxides is suppressed, as evidenced by the absence of iron oxide nodules. This occurs because Cr_2O_3 and Al_2O_3 predominate over iron-oxide in the transient scale and Cr_2O_3 provides oxygen to the alloy much slower than the iron-oxides, which have higher dissociation pressures. Thus, aluminum diffusion up to the surface is facilitated, producing a protective Al_2O_3 layer immediately beneath the thin transient scale.

The reasons this duplex morphology is more protective than the single Al_2O_3 layer are not known. However, their protective nature might

be attributed to several factors: (1) The duplex layer of Cr_2O_3-Al_2O_3 is less susceptible to fracture. (2) The concentration of chromium and aluminum in the vicinity of any fracture that does occur is sufficient so that the nucleation of the iron-rich oxide is suppressed. (3) The formation of the healing Cr_2-O_3-Al_2O_3 scale might be so fast that iron-rich oxides do not nucleate.

The Fe-(5, 10, 15)Cr-10Al and Fe-18Cr-7Al alloys contained sufficient aluminum to form an external Al_2O_3 scale without first forming a thin transient surface film of Cr_2O_3. Due to the presence of chromium the level of aluminum available in these ternary alloys was sufficient to form a healing layer of Al_2O_3 when scale fracture occurred. However, with multiple ruptures of the Al_2O_3 film, the aluminum concentration was depleted below the critical level where a continuous healing Al_2O_3 scale ceased to form.

Thermodynamics, oxidation kinetics and the bulk alloy composition determine the phases formed on the alloy surface during oxidation. A Fe-Al alloy containing a minimum concentration of 7 wt % Al forms an external scale of Al_2O_3 in an oxygen-bearing environment. Although Al_2O_3 has the largest negative free energy of formation, additional oxide phases will form should the level of aluminum drop below the critical concentration. The presence of several oxide layers on the Fe-10Al alloy (Figure 8) and Fe-(5, 10, 15)Cr-10Al alloys suggests that a repetitive process of rupture and growth of the scale occurred. Due to this cyclic process, the aluminum concentration at the surface of these alloys was depleted to a level which was unable to suppress the nucleation and rapid growth of the iron-rich oxide phase. Consequently,

on these alloy surfaces, nodules of iron-rich oxide were observed.

The scanning electron micrograph in Figure 4 shows the presence of small depressions in a region of the alloy surface beneath the Al_2O_3 scale. The formation of these cavities resulted from the outward diffusion of cations during the oxidation of the alloy[18, 19, 20]. Vacancies were created when metallic ions left the metal matrix and migrated to the alloy-oxide junction. There they formed microscopic voids. Voids resulted in the loss of contact between scale and substrate and promoted the formation of a perforated oxide film.

The adherence of the oxide layer determines to a large extent the protective properties of the scale. The formation of voids greatly decreases the adhesion of the oxide to the alloy substrate, as large voids in the remaining metal may become completely disconnected from the oxide. This porosity does not in itself cause the oxide to cease to be protective but the mechanical strength of the oxide layer is small without the support of the metallic substrate.

Scale adherence seemed to be greatest for those alloys that developed the smooth and compact structure. The oxide which developed as a spaghetti-like structure detached easily from the metal substrate. Examination of the Fe-(5, 10, 15)Cr-10Al alloys in cross-section showed, in some instances, the presence of internal inclusions of Al_2O_3 below a thin, adherent surface scale of Al_2O_3 (Figure 7a). In the alloys where internal precipitates of Al_2O_3 were absent, the Al_2O_3 layer was not attached to the metal substrate. Two mechanisms have been proposed to explain the increase in adherence of the external oxide layer. The internal inclusions of oxide act to "key" the surface film to the metal substrate[21] or

internal oxide inclusions below the alloy-oxide interface act as sinks or vacancies, thus eliminating the formation of pores[22]. An increase in the adhesion of the oxide to the alloy substrate is, therefore, realized.

The observed spaghetti-like morphology might have occurred during scale growth due to stress accommodation or during cooling of the oxidized samples from furnace temperature due to large differences in the thermal expansion of the Al_2O_3 and the alloy[23]. The spaghetti-like morphology was always observed on the surface of the binary alloy oxidized in air, but not always on the other Fe-Cr-Al alloys. Small amounts of chromium or Cr_2O_3 in the Al_2O_3 scale may have acted to decrease the plasticity of the Al_2O_3 scale.

Intuition suggests that reducing the oxygen partial pressure at the surface should reduce the flux of oxygen to the metal interior. Therefore, the extent of internal oxidation would be expected to be less in those alloys oxidized in the low P_{O_2} environment. Comparison of the cross-section of the alloys exposed for three days in the two different atmospheres showed that the depth of penetration of oxides into the metal substrate was greater for the air-oxidized specimens.

CONCLUSIONS

The results presented above allow the following conclusions to be drawn:

1. The formation of oxide scales in air on the surfaces of the Fe-Cr-Al alloys appeared to obey a parabolic rate law.

2. The effect of the oxygen partial pressure on the oxidation

morphology was most noticeable in the case of the Fe-10Al. The effect of the P_{O_2} was less noticeable on the Fe-Cr-Al alloys. In the low P_{O_2} atmosphere the formation of a non-protective surface scale of Al_2O_3 allowed extensive internal oxidation of the binary alloy.

3. The oxidation morphology of the Fe-(5, 10, 15)Cr-10Al alloys was dependent upon the experimental technique.

4. A convoluted scale morphology occurred in the absence of inclusions of Al_2O_3 below the surface Al_2O_3 scale. A more adherent surface scale was obtained with internal Al_2O_3 precipitates.

5. Formation of depressions in the alloy surface promoted a non-adherent surface oxide layer.

6. Chromium as an alloying element had a considerable effect on the oxidation rate of the Fe-(5, 10, 15)Cr-10Al alloys. Increasing oxidation resistance was obtained with increasing concentrations of chromium.

7. The alloys which had the best oxidation resistance were Fe-18Cr-3Al and Fe-18Cr-5Al. The adherent oxide layer and excellent scaling resistance were attributed to the formation of a duplex Cr_2O_3-Al_2O_3 scale.

ACKNOWLEDGEMENTS

This work was supported by the Division of Materials Sciences, Office of Basic Energy Sciences, U. S. Department of Energy under contract No. W-7405-ENG-48. The authors gratefully acknowledge the assistance given by the support staff of MMRD.

REFERENCES

1. A. J. McNab, Chemical Engineering Progress, 71, No. 11 (November, 1977).

2. A. G. Gray, Metals Progress, 113, No. 5 (May, 1976).

3. F. C. Schorra and J. G. Pate, "Design Considerations for low-BTU Coal Gasification," presented at the American Society for Metals Conference on Materials for Coal Conversion Systems Design, Chatham Center, Pittsburgh, PA (April, 1976).

4. W. W. Bodle and K. C. Vyas, The Oil and Gas Journal (August, 1974).

5. R. R. Irving, Iron Age, 213 (1974).

6. G. R. Wallwork and A. Z. Hed, Oxidation of Metals, 3, No. 2 (1971), pp. 171-184.

7. J. L. Smialek, Met. Trans., 9A, No. 3 (March, 1978) pp. 309-320.

8. R. B. Mundhe, M.S. Thesis and K. M. Wang, M.S. Thesis, Department of Materials Science and Mineral Engineering, University of California, Berkeley (1978).

9. G. Wagner, Corrosion Science, 5, No. 11 (1965) pp. 751-764.

10. I. A. Kvernes and P. Kofstand, Met. Trans., 3 (June, 1972) pp. 1511-1519.

11. V. Nagarajan and A. V. Levy, LBL-7331 (May, 1978).

12. C. S. Giggins and F. S. Pettit, Journal of the Electrochemical Society, 118, No. 11 (November, 1971) pp. 1782-1790.

13. I. G. Wright and B. A. Wilcox, Oxidation of Metals, 8, No. 5 (1974).

14. G. C. Wood and D. P. Whittle, Corrosion Science, 4, No. 3 (1964).

15. F. H. Stott, G. C. Good and M. G. Hobby, Oxidation of Metals, 3, No. 2 (1971).

16. G. C. Wood, Oxidation of Metals, 2, No. 1 (1970).

17. G. C. Wood, Corrosion Science, 2, No. 3 (1961).

18. J. Pappis and W. D. Kingery, J. Am. Ceram. Soc., 44, (1961) p 459.

19. A. E. Paladino and W. D. Kingery, J. Am. Ceram. Soc., 37 (1962) p. 957.

20. T. D. Jones, R. L. Coble and C. J. Mogab, J. Am. Ceram. Soc., 52, (1969) p. 331.

21. D. P. Whittle, M. E. El Dahshan and J. Stringer, Corrosion Science, 17, No. 11 (1977) pp. 879-891.

22. J. Stringer, personal communication to A. U. Seyboh (1966).

23. J. Stringer and D. P. Whittle, Revs. Int. Htes. Temp. et Refrac., 14, No. 6 (1977).

FIGURE CAPTIONS

FIGURE 1 (a) and (b) Kinetics obtained for oxidation in air at 982°C (1800°F) of the Fe-18Cr-Si Alloys.

FIGURE 2 Scanning micrograph showing the morphological features developed on the Fe-18Cr-7Al alloy

(a) Numerous wrinkles formed during oxidation in air at 982°C are evident in the Al_2O_3 scale.

(b) Region where the Al_2O_3 surface scale detached from the alloy substrate.

FIGURE 3 Scanning micrograph showing the morphological feature developed on the Fe-10Cr-10Al alloy. A smooth oxide layer formed in the low P_{O_2} atmosphere at 982°C. Nodules of Al_2O_3 protrude through the Al_2O_3 surface layer.

FIGURE 4 Scanning micrograph showing the Al_2O_3 surface morphology during oxidation for five days in air at 982°C (1800°F)

(a) Fe-10Al
(b) Fe-10Cr-10-Al
(c) Fe-18Cr-3Al

FIGURE 5. Scanning micrograph showing a region where spalling occurred. A region of the alloy surface was exposed showing depressions in the alloy surface. This sample of Fe-5Cr-10Al was oxidized in air for five days at 982°C.

FIGURE 6. Scanning micrograph showing the morphological features developed on the Fe-10Al alloy during oxidation.

(a) The ballooned and convoluted structure of Al_2O_3 formed during oxidation in air at 982°C (1800°F).

(b) The fine, granular texture of Al_2O_3 formed during oxidation in the low P_{O_2} atmosphere (P_{O_2} = 10^{-18} atm) at 982°C (1800°F).

In both (a) and (b) nodules of a complex iron-rich oxide protrude through the surface Al_2O_3 scale.

FIGURE 7. Optical micrograph showing the internal formati on of Al_2O_3 inclusions.

(a) Fe-5Cr-10Al oxidized in air for five days at 982°C (1800°F).

(b) Fe-15Cr-10Al oxidized in air for five days at 982°C (1800°F).

FIGURE 8. Scanning micrograph showing the morphology in cross-section developed during oxidation in air at 982°C (1800°F).

(a) Fe-10Cr-10Al exposed for five days in the box furnace.

(b) Fe-5Cr-10Al exposed for five days in the tube furnace.

FIGURE 9. Scanning micrograph showing the morphology of Fe-10Al in cross-section. The ballooned and convoluted oxide structure formed during five days in air at 982°C (1800°F).

FIGURE 10. (a) Scanning micrograph showing the morphology in cross-section of the Fe-10Al alloy after oxidation in the low P_{O_2} atmosphere at 982°C for three days.

(b) Iron x-ray map.

(c) Aluminum x-ray map.

FIGURE 11. (a) Scanning micrograph at a higher magnification of an area shown in Figure 10.

(b) Iron x-ray map.

(c) Aluminum x-ray map.

TABLE I

ALLOY COMPOSITION (IN WT %)

Alloy Nominal Composition	Actual Composition		
	Fe	Cr	Al
Fe-10Al	Bal.	----	9.29
Fe-5Cr-10Al	Bal.	4.91	9.03
Fe-10Cr-10Al	Bal.	14.64	9.21
Fe-15Cr-10Al	Bal	16.83	8.76
Fe-18Cr-3Al	Bal.	17.56	2.56
Fe-18Cr-5Al	Bal.	17.74	3.34
Fe-18Cr-7Al	Bal.	17.64	6.64

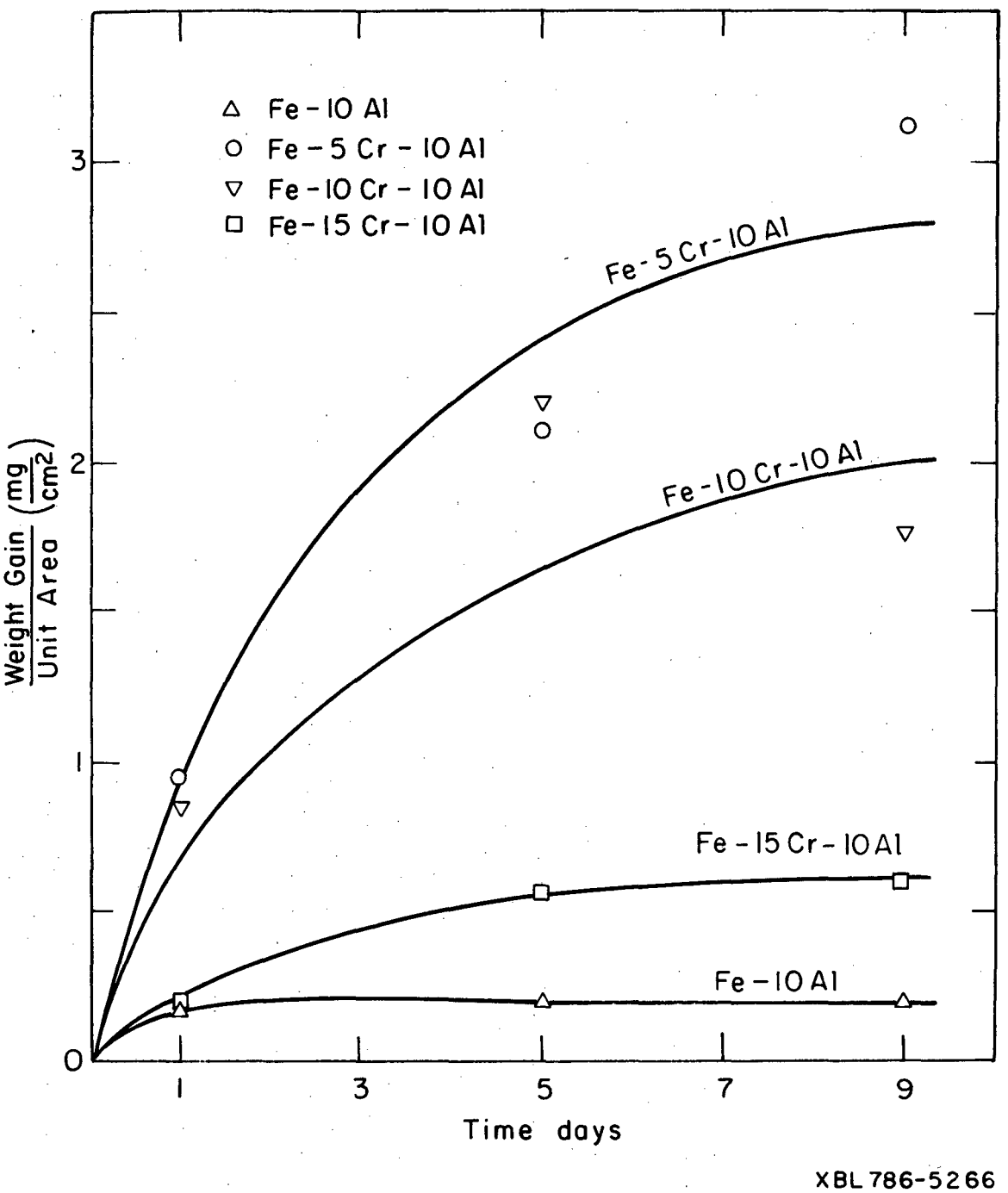
Fe - 10 Al
Fe - 5 Cr - 10 Al
Fe - 10 Cr - 10 Al
Fe - 15 Cr - 10 Al
Fe - 5 Cr - 10 Al
Fe - 10 Cr - 10 Al
Fe - 15 Cr - 10 Al
Fe - 10 Al
Weight Gain / Unit Area (mg/cm²)
0
1
2
3
1
3
5
7
9
Time days
XBL 786-5266

FIGURE 1(a).

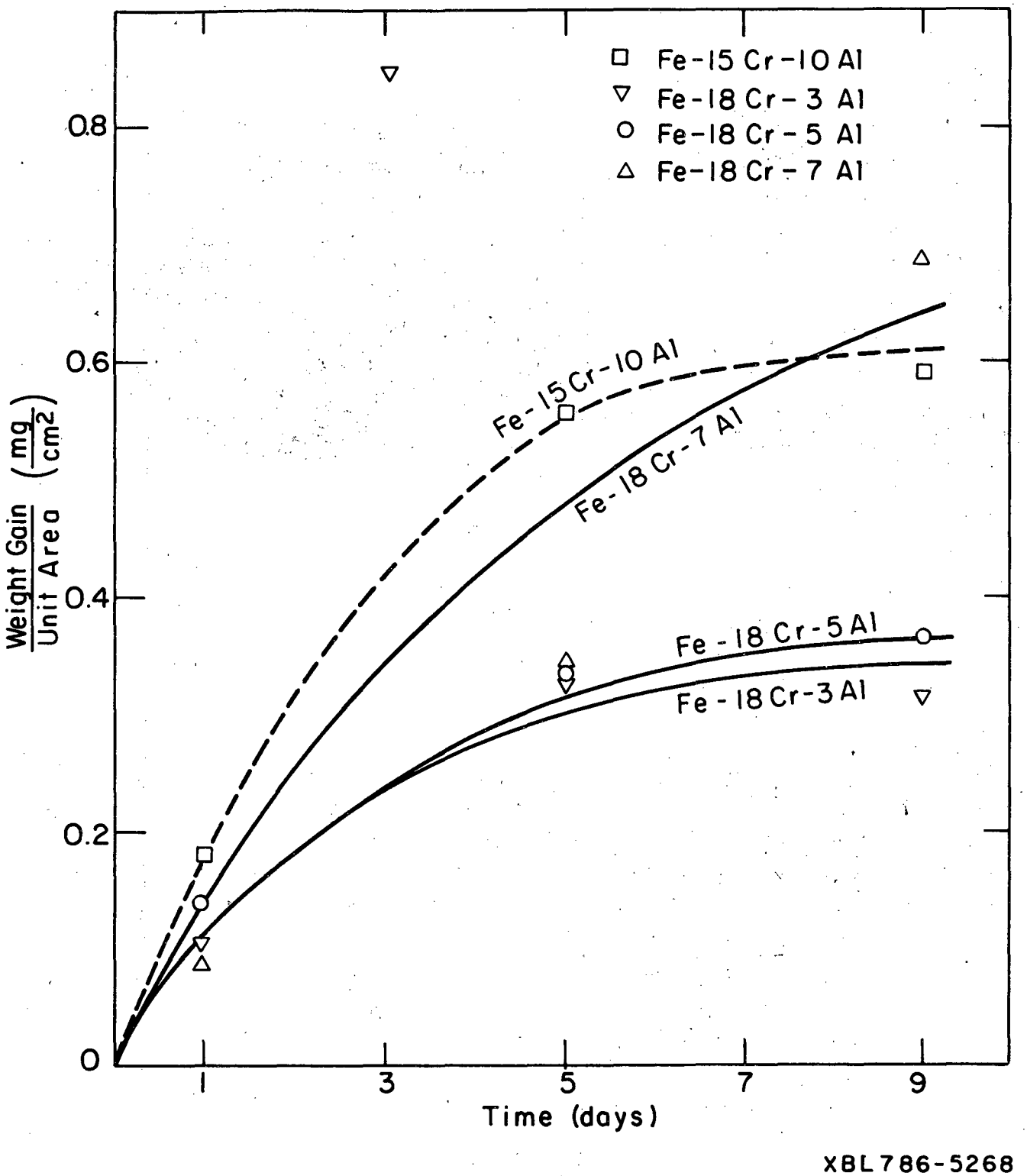
Fe-15 Cr-10 Al
Fe-18 Cr-3 Al
Fe-18 Cr-5 Al
Fe-18 Cr-7 Al
Fe-15Cr-10 Al
Fe-18 Cr-7 Al
Fe-18 Cr-5 Al
Fe-18 Cr-3 Al
Weight Gain / Unit Area (mg/cm²)
0
0.2
0.4
0.6
0.8
1
3
5
7
9
Time (days)
XBL786-5268

FIGURE 1 (b).

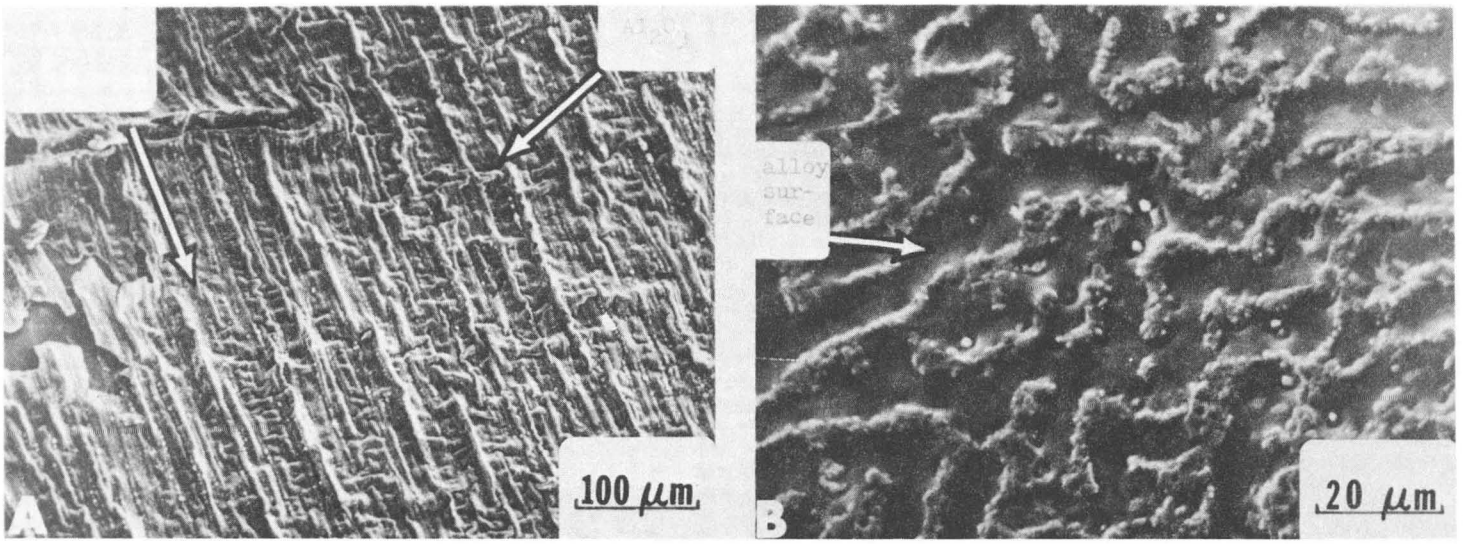

FIGURE 2.

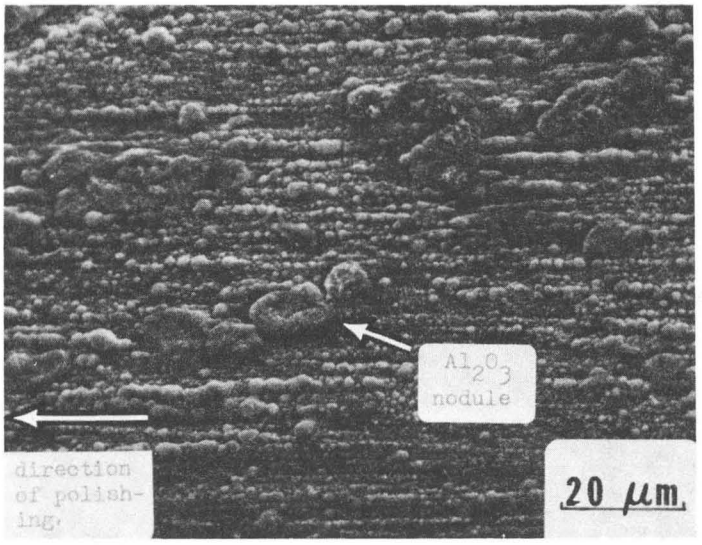

FIGURE 3.

XBB 789-10642

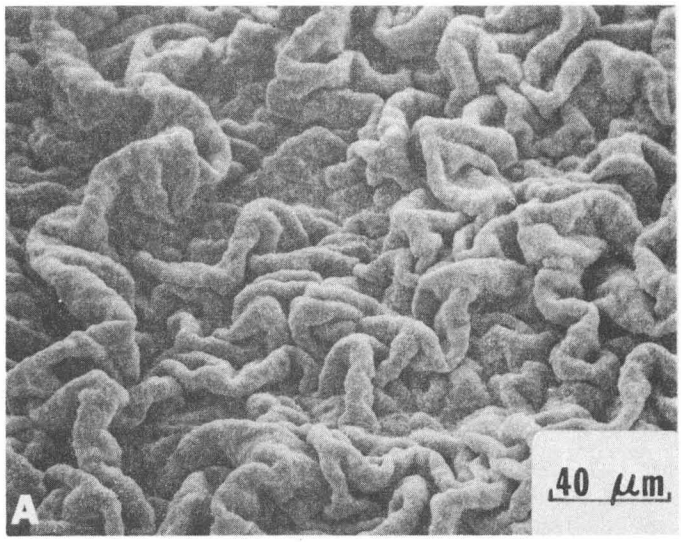

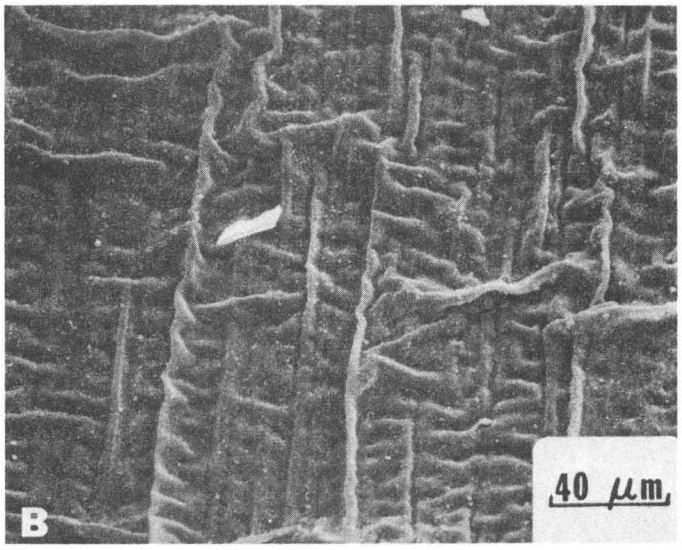

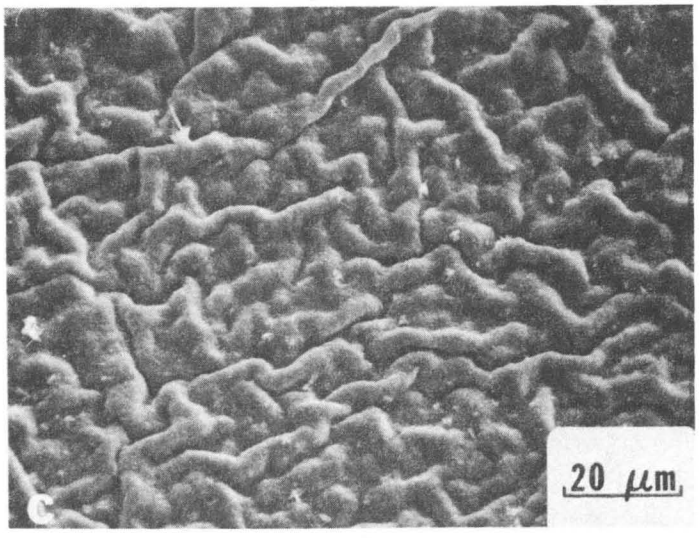

FIGURE 4.

XBB 789-10640

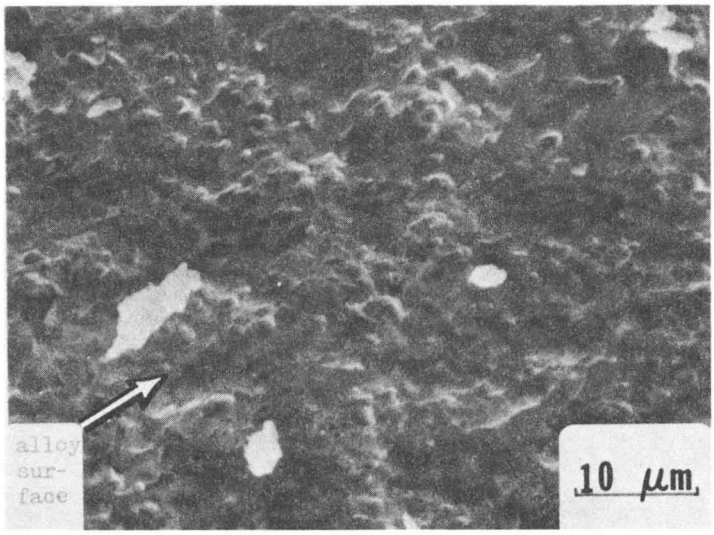

FIGURE 5.

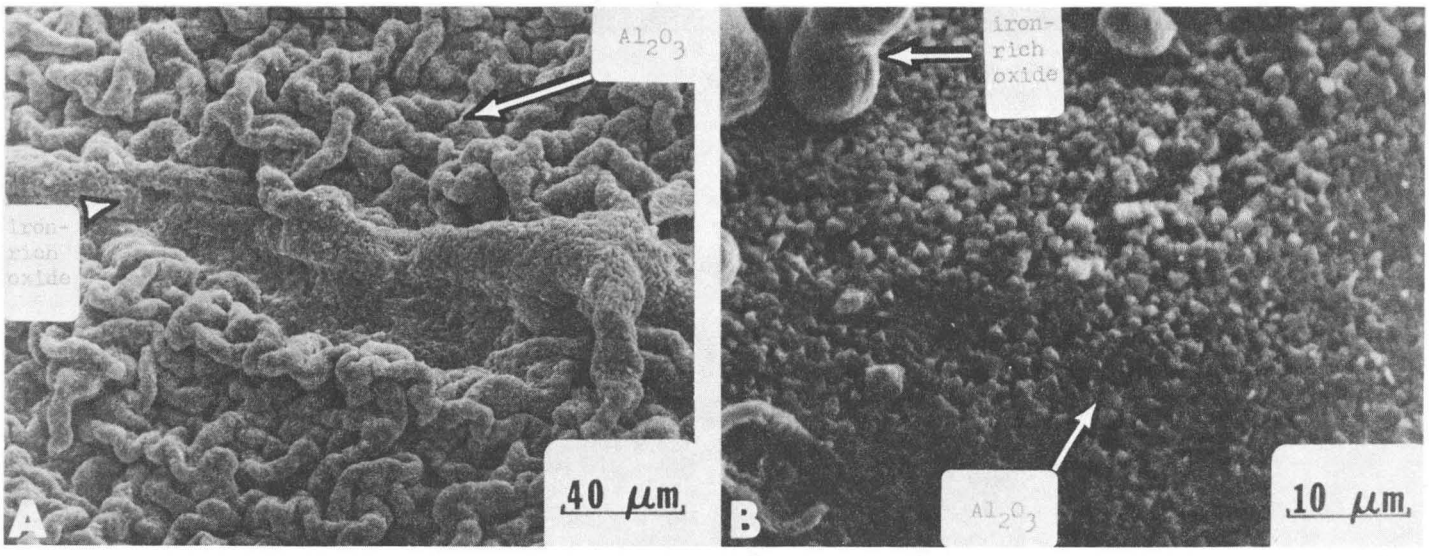

FIGURE 6.

XBB 789-10641

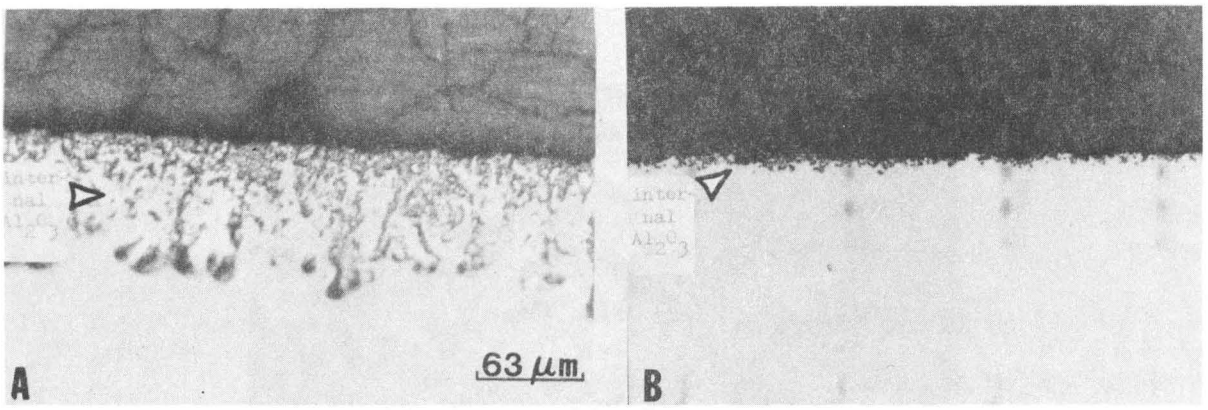

FIGURE 7.

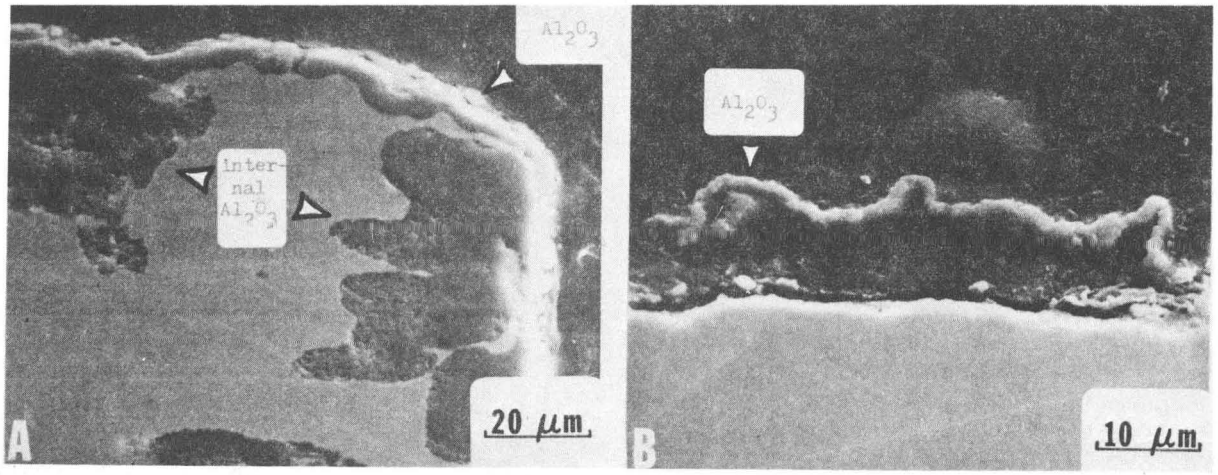

FIGURE 8.

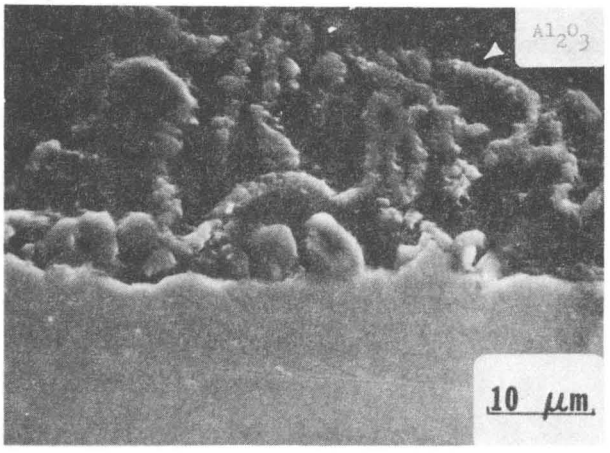

FIGURE 9.

XBB 789-10643

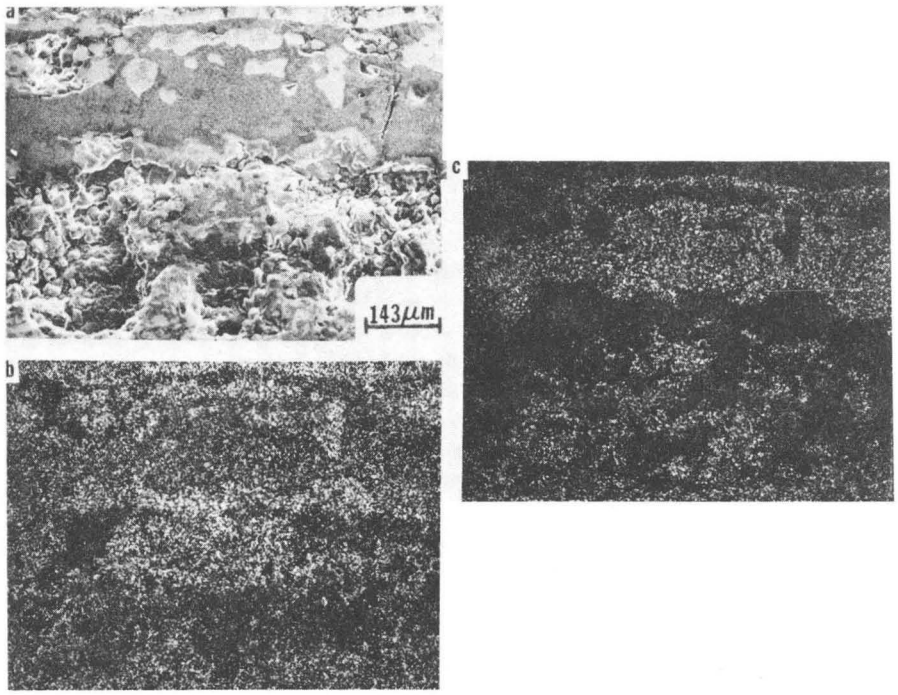

FIGURE 10.

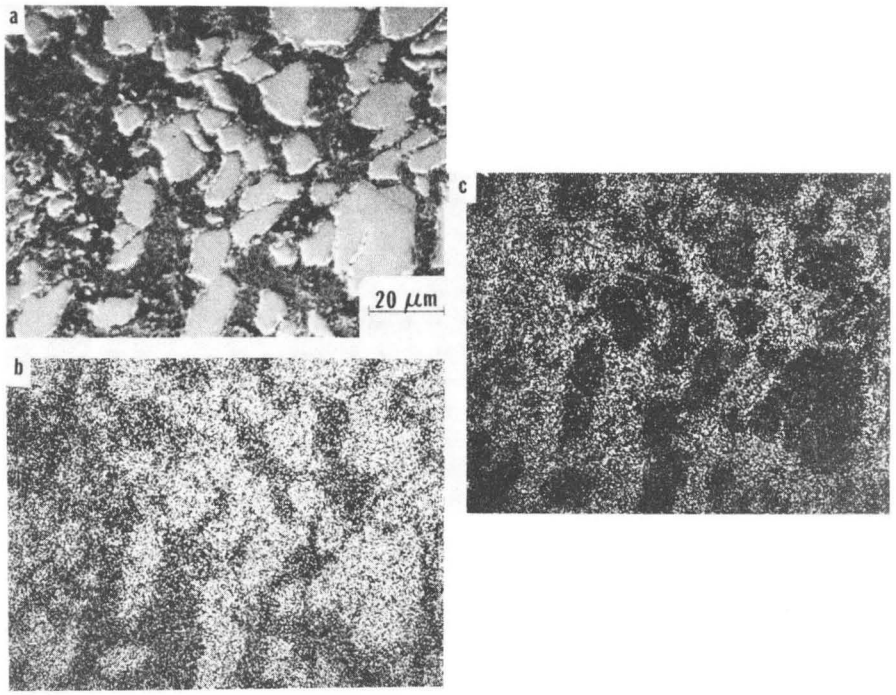

FIGURE 11.

XBB 787-8549

This report was done with support from the Department of Energy. Any conclusions or opinions expressed in this report represent solely those of the author(s) and not necessarily those of The Regents of the University of California, the Lawrence Berkeley Laboratory or the Department of Energy.

Reference to a company or product name does not imply approval or recommendation of the product by the University of California or the U.S. Department of Energy to the exclusion of others that may be suitable.

TECHNICAL INFORMATION DEPARTMENT
LAWRENCE BERKELEY LABORATORY
UNIVERSITY OF CALIFORNIA
BERKELEY, CALIFORNIA 94720